Electronic Supplementary Information

H/D isotope effect on the molar volume and thermal expansion of benzene

A. D. Fortes, S. C. Capelli

[1]ISIS Facility, STFC Rutherford Appleton Laboratory, Harwell Science and Innovation Campus, Chilton, Didcot, Oxfordshire, OX11 0QX, U.K.

Corresponding author email: dominic.fortes@stfc.ac.uk

Supplementary Figures

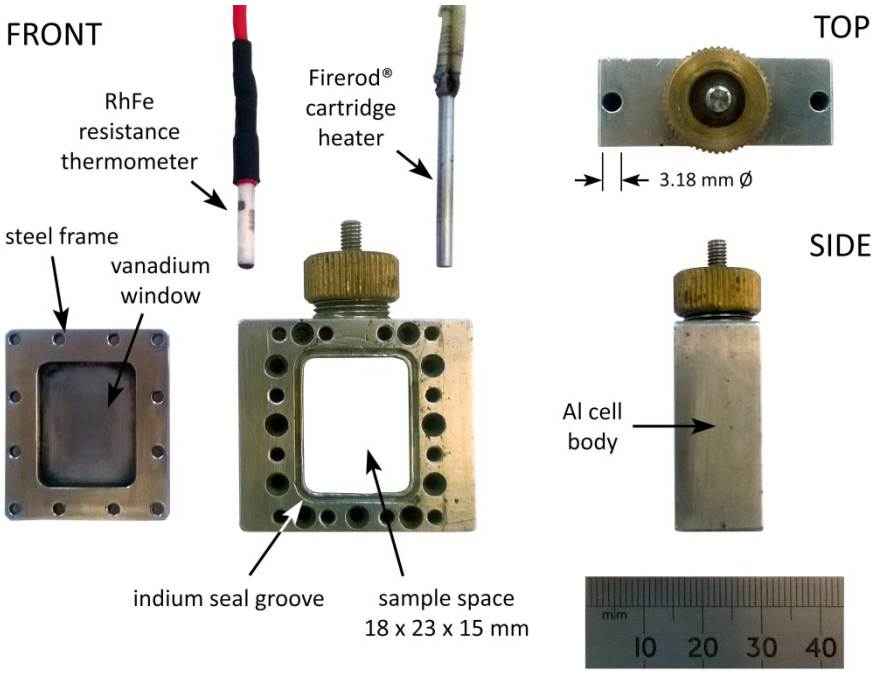

Figure S1: The *in-situ*-heated slab-geometry sample holders used in this work.

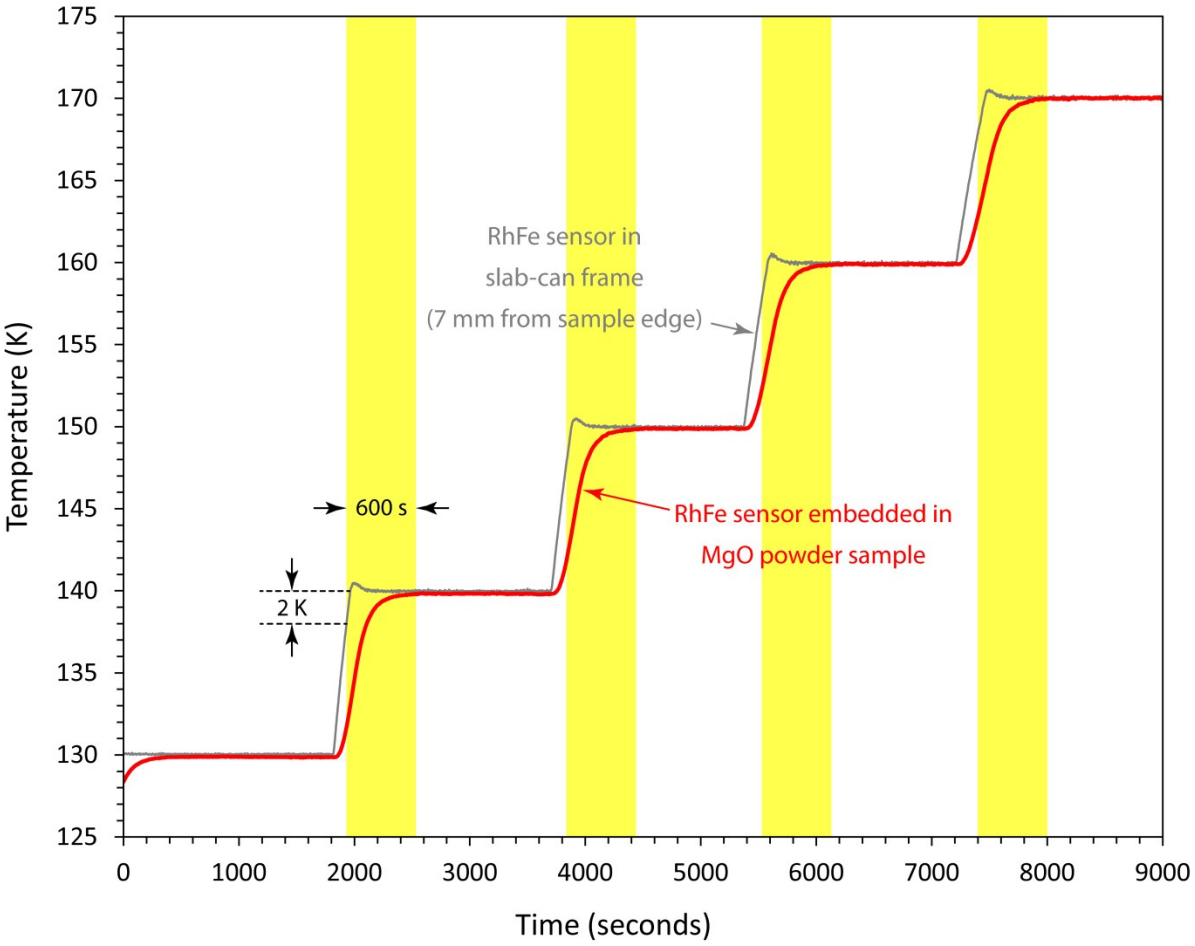

Figure S2: The result of offline testing using a 15 mm-deep slab can containing MgO powder with a RhFe sensor embedded in the centre. The grey line shows the temperature measured by a RhFe sensor in the Al-alloy frame of the can (the typical measurement made during a 'real' experiment) and the red-line is the measured temperature in the middle of the MgO powder. Yellow bands indicate a 10 minute period after the frame sensor is within 2 K of the set-point. In the absence of an embedded sensor in 'live' online experiment, pursuit of this strategy – slow-ramp and equilibration wait – provides a degree of certainty that the sample temperature is both an accurate and precise reflection of the sample holder's temperature.

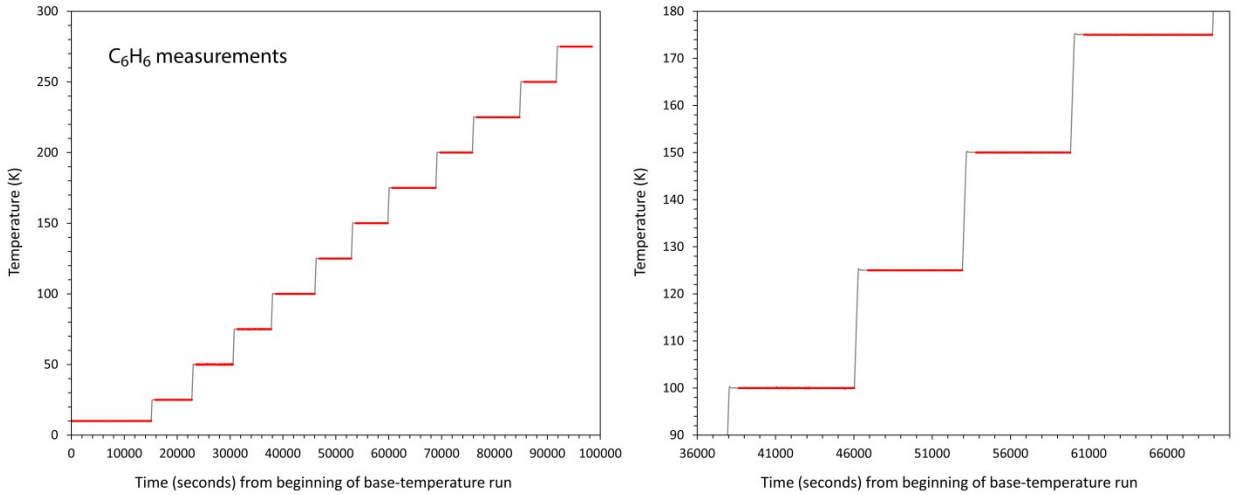

Figure S3: Plot of the logged frame temperatures during our C_6H_6 measurements. The grey line contains the complete thermal record and the red segments indicate where in this record the data collection occurred. Note that the measurements are much longer than with C_6D_6, leading to the equilibration times appearing very short by comparison with the subsequent 100 minute time-of-flight data collection (in reality, the same 10 minute wait was used).

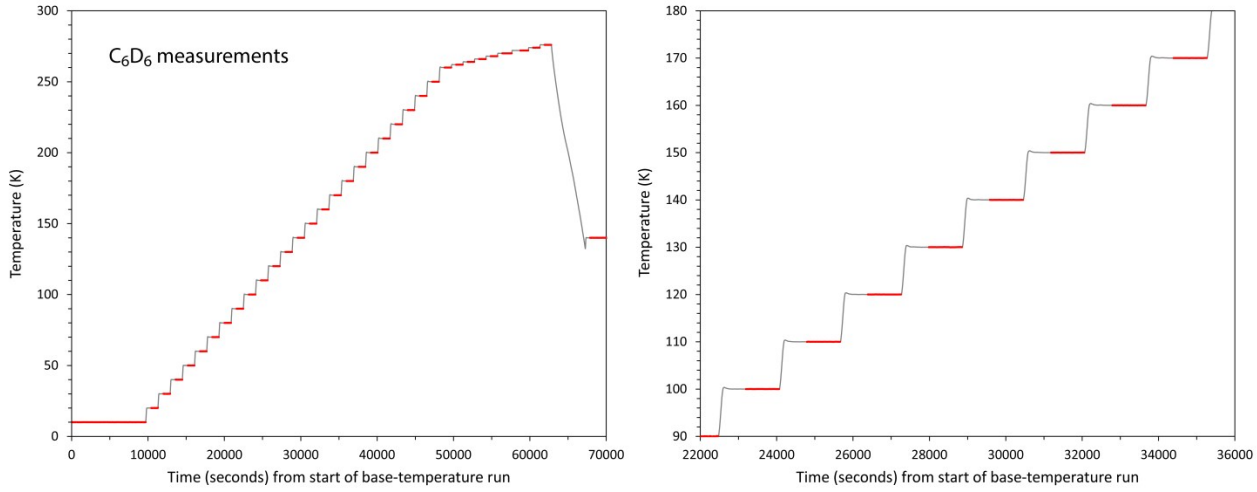

Figure S4: Plot of the logged frame temperatures during our C_6D_6 measurements, where lines and colours have the same meaning as in Figure S3.

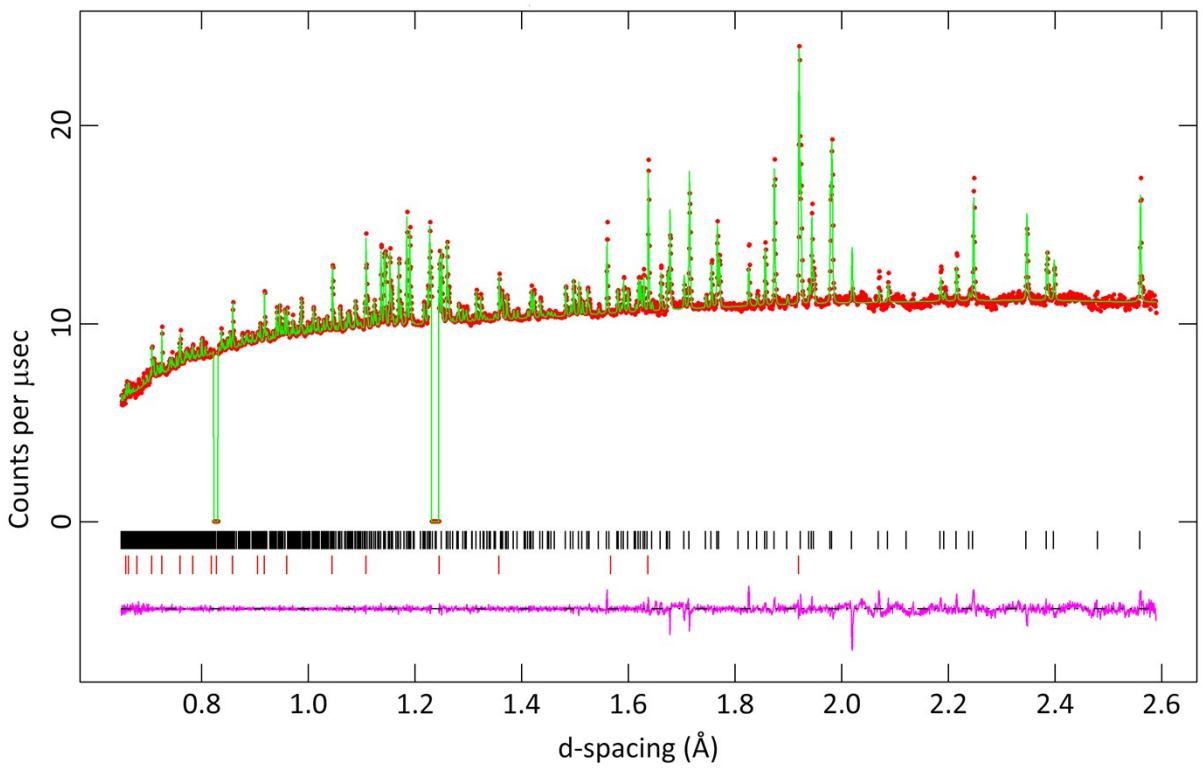

Figure S5

High-resolution neutron powder diffraction data for C_6H_6 measured at 10 K collected in backscattering using a 30–130 ms time-of-flight window. Filled red circles are the data and the solid-green line is an 'F(Calc) weighted' fit, the difference curve being reported in purple underneath. Vertical tick marks show the positions of Bragg reflections from C_6H_6 (top) and silicon (bottom). The two excluded regions at shorter d-spacings are due to removal of prompt-pulse artefacts (see main text). Note that the overall count rate is around an order of magnitude lower than from the deuterated sample and that the signal sits on top of a substantial incoherent background due to ^{1}H.

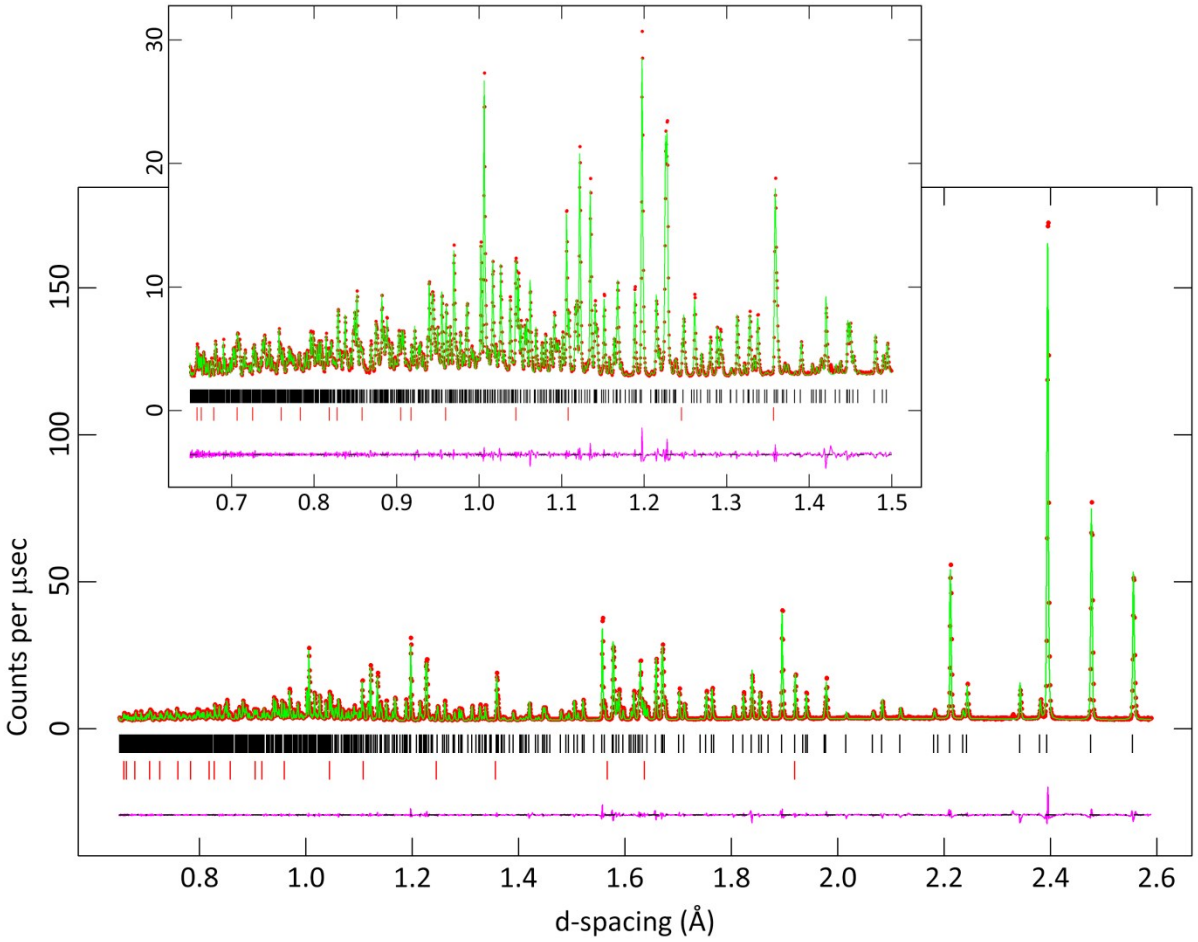

Figure S6a

High-resolution neutron powder diffraction data for C_6D_6 measured at 10 K using a 30–130 ms time-of-flight window. Filled red circles are the data and the solid-green line is an 'F(Calc) weighted' fit, the difference curve being reported in purple underneath. Vertical tick marks show the positions of Bragg reflections from C_6D_6 (top) and silicon (bottom).

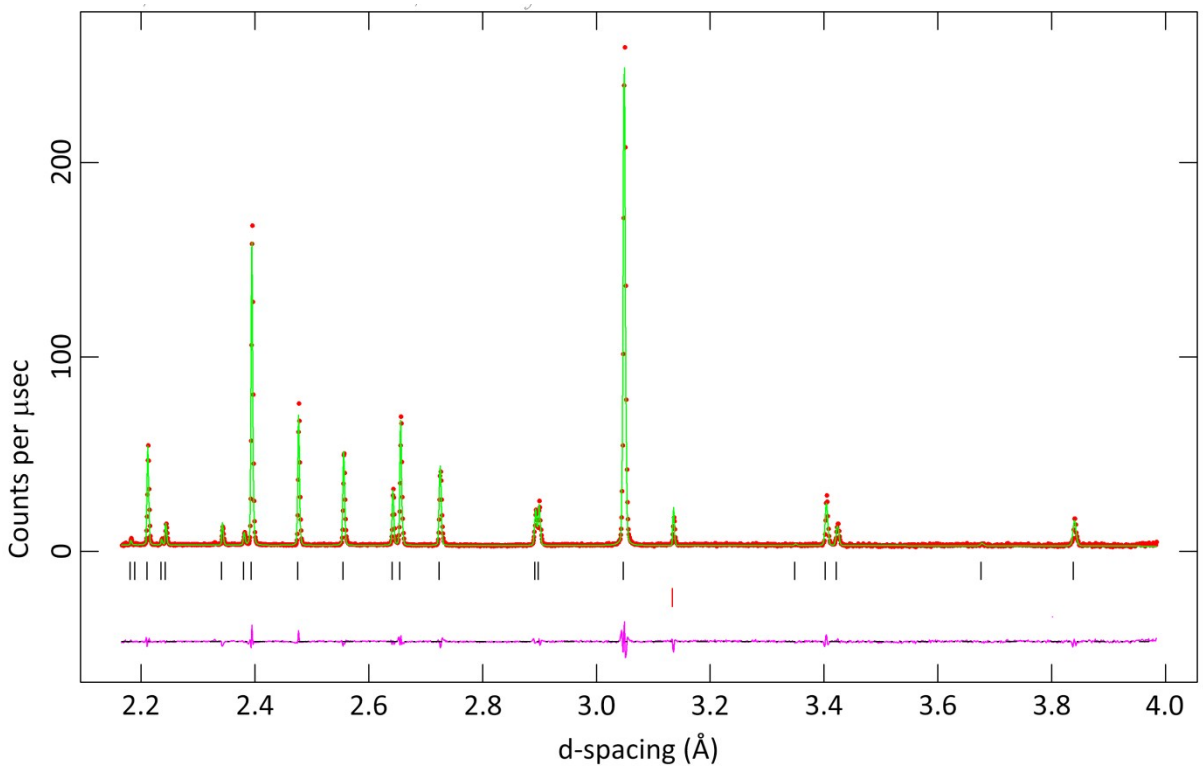

Figure S6b

High-resolution neutron powder diffraction data for C_6D_6 measured at 10 K using a 100–200 ms time-of-flight window. Filled red circles are the data and the solid-green line is an 'F(Calc) weighted' fit, the difference curve being reported in purple underneath. Vertical tick marks show the positions of Bragg reflections from C_6D_6 (top) and silicon (bottom).

All of the raw experimental data can be accessed at doi: 10.5286/ISIS.E.87846762 (2017).

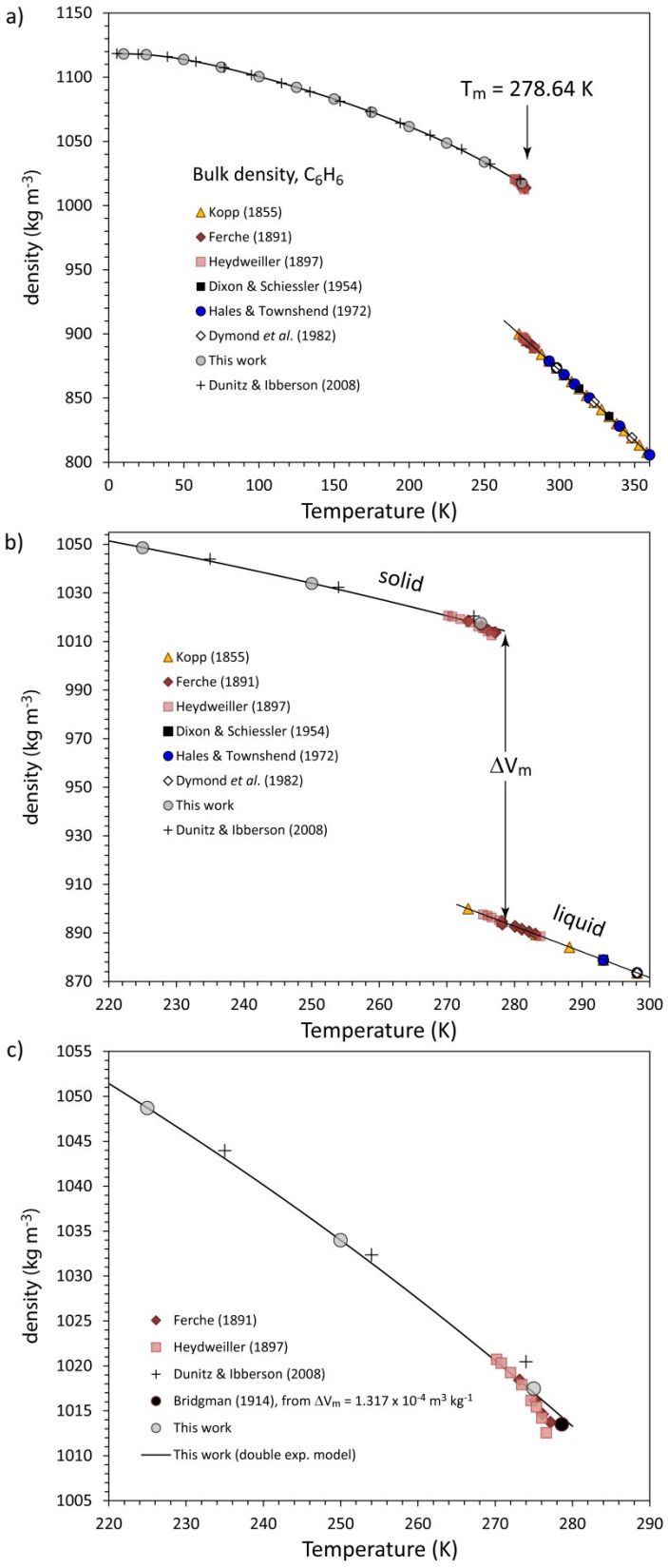

Figure S7

Compilation of density measurements for ordinary benzene in its liquid and crystalline solid form compared with densities calculated from unit-cell volumes obtained by neutron powder

diffraction. The literature measurements agree very well with one another, with the exception of the two oldest works: Kopp (1855) reports liquid densities that are systematically 0.1 % smaller than all later values; Ferche (1891) reports liquid *and* solid densities that are systematically 0.75 % smaller than all later values. For the purpose of this illustration, both Kopp's and Ferche's densities have been adjusted upward by 0.1 and 0.75 %, respectively. A 2nd-order polynomial was fitted through the liquid densities in the range 270 – 360 K in order to find an accurate value for the density of the liquid at the melting point. The density of the solid at the melting point was found using the double-exponential model fitted to the lattice parameters (see main text).

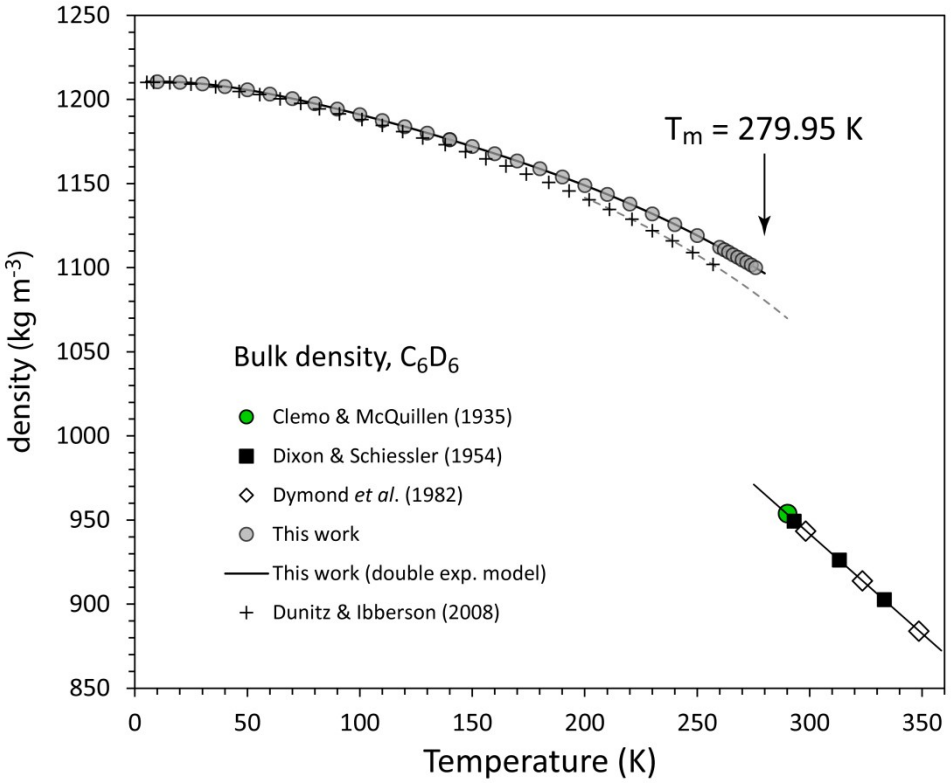

Figure S8

Compilation of density measurements for perdeuterated benzene in its liquid and crystalline solid form. As for C_6H_6, a second-order polynomial was fitted to the literature-derived liquid density data and the density of the solid at the melting point was extrapolated using our double-exponential model fit. The dashed grey line show likely variation of density up to the melting point based in the measurements of Dunitz & Ibberson (2008).

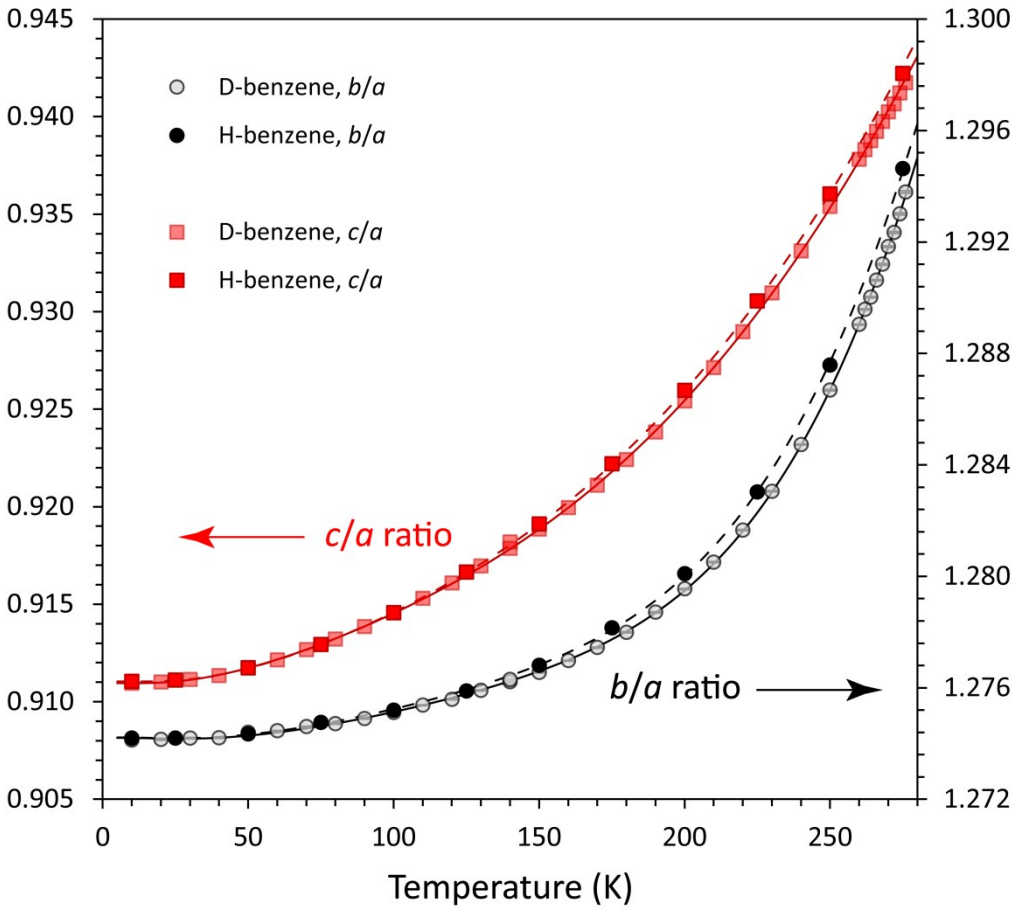

Figure S9

Axial ratios, *b*/*a* in black and *c*/*a* in red, for both isotopologues. Solid lines report the trends for C_6D_6 from fitting of Eqs. 1 and 2 to the unit-cell parameters and dashed lines report the same results for C_6H_6.

Supplementary Tables

Table S1: Unit-cell parameters of C_6H_6 as a function of temperature. Uncertainties in T are the standard deviation of the measured temperature during the period in which data was being collected. Uncertainties in the cell parameters and the volume are those reported by GSAS.

T (K)	*a* (Å)	*b* (Å)	*c* (Å)	V (Å^3)
10.00(2)	7.36623(4)	9.38602(5)	6.71088(4)	463.987(3)
24.99(4)	7.36749(6)	9.38756(7)	6.71250(5)	464.255(5)
50.0(1)	7.37376(7)	9.39672(7)	6.72284(5)	465.820(5)
75.00(7)	7.38301(6)	9.41150(8)	6.74017(6)	468.342(5)
99.99(2)	7.39423(7)	9.42905(9)	6.76245(6)	471.482(5)
125.00(1)	7.40580(6)	9.44895(8)	6.78844(5)	475.035(5)
150.01(1)	7.41818(7)	9.4715(1)	6.81811(6)	479.051(6)
175.00(1)	7.43065(7)	9.4975(1)	6.85249(7)	483.596(5)
200.01(1)	7.44306(8)	9.5278(1)	6.89193(7)	488.747(6)
225.00(1)	7.45531(9)	9.5654(1)	6.93753(9)	494.735(8)
250.00(1)	7.4670(1)	9.6144(2)	6.9893(1)	501.77(1)
275.00(1)	7.4771(2)	9.6801(2)	7.0450(2)	509.91(2)

Table S2: Unit-cell parameters of C_6D_6 as a function of temperature. Uncertainties in T are the standard deviation of the measured temperature during the period in which data was being collected. Uncertainties in the cell parameters and the volume are those reported by GSAS. Data were collected on warming from 10 to 276K; the final point at 140 K was measured after cooling back down from 276 K.

T (K)	*a* (Å)	*b* (Å)	*c* (Å)	V (Å^3)
10.01(2)	7.35438(2)	9.37040(2)	6.69943(2)	461.681(1)
20.01(2)	7.35482(8)	9.37111(8)	6.70030(7)	461.804(4)
30.00(3)	7.35633(8)	9.37340(8)	6.70268(7)	462.176(4)
39.99(2)	7.35907(8)	9.37696(9)	6.70652(7)	462.788(4)
50.01(3)	7.36168(8)	9.38170(8)	6.71202(7)	463.566(4)
60.00(2)	7.36549(8)	9.38696(8)	6.71840(6)	464.507(4)
70.00(3)	7.36945(7)	9.39313(8)	6.72586(6)	465.579(4)
80.00(3)	7.37386(7)	9.39953(8)	6.73391(6)	466.733(4)
90.00(3)	7.37833(7)	9.40659(8)	6.74264(6)	467.973(4)
100.00(1)	7.38288(7)	9.41403(8)	6.75212(6)	469.290(4)
110.00(1)	7.38768(6)	9.42207(8)	6.76194(5)	470.680(4)
120.00(1)	7.39262(7)	9.42990(9)	6.77227(6)	472.106(5)
130.01(2)	7.39758(6)	9.43862(8)	6.78323(5)	473.625(4)
140.00(1)	7.40277(6)	9.44751(8)	6.79465(6)	475.203(4)
150.01(1)	7.40808(7)	9.45680(8)	6.80687(6)	476.867(4)
160.00(1)	7.41328(6)	9.46656(8)	6.81977(6)	478.599(4)
170.00(1)	7.41860(6)	9.47682(9)	6.83326(6)	480.411(4)
180.03(2)	7.42388(7)	9.48766(9)	6.84782(6)	482.328(5)
190.01(2)	7.42905(7)	9.49958(9)	6.86318(6)	484.354(5)
200.00(1)	7.43406(7)	9.51224(9)	6.87955(6)	486.484(5)
210.00(1)	7.43920(6)	9.52596(9)	6.89705(6)	488.763(5)
220.01(1)	7.44421(7)	9.5409(1)	6.91545(7)	491.168(5)
230.01(1)	7.44920(7)	9.5577(1)	6.93487(6)	493.744(5)
240.01(1)	7.45403(6)	9.5764(1)	6.95544(6)	496.500(5)
250.01(1)	7.45878(7)	9.5971(1)	6.97692(7)	499.426(6)
260.00(1)	7.46339(7)	9.6206(1)	6.99924(7)	502.561(6)
262.00(1)	7.46439(8)	9.6259(1)	7.00381(7)	503.235(6)
264.00(1)	7.46553(9)	9.6307(1)	7.00831(8)	503.883(7)
265.99(2)	7.4665(1)	9.6364(1)	7.01282(9)	504.574(7)
268.00(1)	7.4674(1)	9.6419(2)	7.01740(9)	505.254(8)
270.01(1)	7.4684(1)	9.6479(2)	7.0221(1)	505.973(8)
272.01(1)	7.4697(1)	9.6534(2)	7.0263(1)	506.65(1)
274.01(1)	7.4704(1)	9.6593(2)	7.0312(1)	507.37(1)
276.01(2)	7.4711(2)	9.6661(2)	7.0358(1)	508.10(1)
139.99(3)	7.40185(6)	9.44693(7)	6.79627(5)	475.227(4)

Table S3: Parameters obtained by least-squares fitting of equations 1 and 2 to the data given in Tables 1 and 2. Not that all parameters were fitted independently for the *b*-axis and *c*-axis; for the *a*-axis, the terms *q* and *s* were fixed equal in the protiated and deuterated species and determined as part of a global fit. RSS = residual sum of squares.

Parameter	C_6D_6	C_6H_6
***a*-axis**		
a_0 (Å)	7.3542(1)	7.3662(1)
p	$9.3(1) \times 10^{-5}$	$9.0(1) \times 10^{-5}$
q	−35.9(8)	−35.9(8)
r	$-2.2(4) \times 10^{-5}$	$-2.5(5) \times 10^{-5}$
s	−652(57)	−652(57)
RSS	7.21×10^{-7}	4.04×10^{-7}
***b*-axis**		
b_0 (Å)	9.3707(2)	9.3861(3)
p	$1.29(2) \times 10^{-4}$	$1.28(2) \times 10^{-4}$
q	−45(1)	−45(1)
r	$2.2(2) \times 10^{-3}$	$1.6(2) \times 10^{-3}$
s	−1288(23)	−1206(35)
RSS	3.70×10^{-6}	9.36×10^{-7}
***c*-axis**		
c_0 (Å)	6.6993(2)	6.7109(1)
p	$2.13(3) \times 10^{-4}$	$2.26(2) \times 10^{-4}$
q	−43.7(9)	−48.3(5)
r	$1.67(9) \times 10^{-3}$	$1.70(5) \times 10^{-3}$
s	−627(15)	−644(12)
RSS	1.43×10^{-6}	4.65×10^{-8}

Complete list of literature cited

Akella, J., & Kennedy, G. C. (1971). Phase diagram of benzene to 35 kbar. *J. Chem. Phys.*, **55**, 793–796.

Albinati, A., & Willis, B. T. M. (1982). The Rietveld method in neutron and X-ray powder diffraction. *J. Appl. Cryst.,* **15**, 361–374.

Arnold, O., & 27 co-authors (2014). Mantid—Data analysis and visualization package for neutron scattering and μSR experiments. *Nucl. Instrum. Methods Phys. Res. A*, **764**, 156–166.

Bacon, G. E., Curry, N. T., & Wilson, S. A. (1964). A crystallographic study of solid benzene by neutron diffraction. *Proc. Royal Soc. London A*., **279**, 98–110.

Bartell, L. S., & Roskos, R. R. (1966). Isotope effects on molar volume and surface tension: simple theoretical model and experimental data for hydrocarbons. *J. Chem. Phys.*, **44**, 457–463.

Bates, F. S., Keith, H. D., & McWhan, D. B. (1987). Isotope effect on the melting temperature of nonpolar polymers. *Macromol.*, **20**, 3065–3070.

Bridgman, P. W. (1914). Change of phase under pressure. I. The phase diagram of eleven substances with especial reference to the melting curve. *Phys. Rev.*, **3**, 153–203.

Clemo, G. R., & McQuillen, A. (1935). Experiments on hexadeuterobenzene. *J. Chem. Soc*. **1935**, 851–855.

Cox, E. G. (1932). The crystalline structure of benzene. *Proc. Royal Soc. London A*., **135**, 491–498.

Cox, E. G. (1958). Crystal structure of benzene. *Rev. Mod. Phys.,* **30**, 159–162.

Cox, E. G., Cruickshank, D. W. J., & Smith, J. A. S. (1958). The crystal structure of benzene at −3° C. *Proc. Royal Soc. London A*., **247**, 1–21.

Craven, C. J., Hatton, P. D., Howard, C. J., & Pawley, G. S. (1993). The structure and dynamics of solid benzene. I. A neutron powder diffraction study of deuterated benzene from 4 K to the melting point. *J. Chem. Phys*., **98**, 8236–8243.

David, W. I. F., Ibberson, R. M., Jeffrey, G. A., & Ruble, J. R. (1992). The crystal structure analysis of deuterated benzene and deuterated nitromethane by pulsed-neutron powder diffraction: A comparison with single crystal neutron diffraction analysis. *Physica B: Cond. Matt.*, **180**, 597–600.

Deffet, L. (1935). Recherches Piézométriques. – I. Influence des hautes pressions sur la température de fusion et la température de transformation des corps organiques. *Bull. Soc. Chim. Belg.,* **44**, 41–96.

Deffet, L., & Vlerick, G. (1942). La mesure des variations de volume au moyen de l'analyse piézométrique. *Bull. Soc. Chim. Belg*., **51**, 237–256.

Dixon, J. A., & Schiessler, R. W. (1954). Synthesis and properties of deuterocarbons. benzene-d6 and cyclohexane-d12. *J. Am. Chem. Soc.* **76**, 2197–2199.

Dunitz, J. D., & Ibberson, R. M. (2008). Is deuterium always smaller than protium? *Angew. Chem. Int. Ed*., **47**, 4208–4210.

Dymond, J. H., Robertson, N. G. J., & Isdale, J. D. (1982) (*p, ρ, T*) for $\{(1-x)C_6H_6 + xC_6D_6\}$ and $\{(1-x)C_6H_6 + xC_6F_6\}$ in the range 298 to 373 K and 0.1 to 400 MPa. *J. Chem. Thermodyn*. **14**, 1149–1158.

Ferche, J. (1891). Ueber einige physikalische Eigenschaften des Benzols. *Ann. Phys.,* **280**, 265–287.

Figuière, P., Fuchs, A. H., Ghelfenstein, M., & Szwarc, H. (1978). Pressure-volume-temperature relations for crystalline benzene. *J. Phys. Chem. Solids*, **39**, 19–24.

Fortes A. D. (2018). Accurate and precise lattice parameters of H_2O and D_2O ice I*h* between 1.6 and 270 K from high-resolution time-of-flight neutron powder diffraction data. *Acta Cryst. B*. **74**, 196–216.

Henderson, S. J., & Speedy, R. J. (1987). Melting temperature of ice at positive and negative pressures. *J. Phys. Chem*., **91**, 3069–3072.

Heydweiller, A. (1897). Die Erstarrungscontraction für einige organische Verbindungen. *Ann. Phys.,* **297**, 527–540.

Huffman, H. M., Parks, G. S., & Daniels, A. C. (1930). Thermal data on organic compounds. VII. The heat capacities, entropies and free energies of twelve aromatic hydrocarbons. *J. Am. Chem. Soc*., **52**, 1547–1558.

Ibberson, R.M. (2009). Design and performance of the new supermirror guide on HRPD at ISIS. *Nucl. Instr. Meth. Phys. Res. A*., **600**, 47–49.

Ibberson, R.M., David, W.I.F., & Knight, K.S. (1992). The high resolution neutron powder diffractometer (HRPD) at ISIS – a user guide. RAL-92-031. Rutherford Appleton Laboratory, U. K. (http://www.isis.rl.ac.uk/crystallography/documentation/HRPDguide).

Jeffrey, G. A., Ruble, J. R., McMullan, R. K., & Pople, J. A. (1987). The crystal structure of deuterated benzene. *Proc. Royal Soc. London A*., **414**, 47–57.

Kitagawa, S., Fujiwara, Y., & Iijima, T. (1996). A negative experimental result for the structural change of benzene crystal in the premelting process. *Jap. J. Appl. Phys.*, **35**, 5787–5789.

Kohzin, V. M. (1954). Kristallicheskaya struktura benzola. *Zh. Fiz. Khim.* **28**, 566–566.

Kopp, H. (1855). Untersuchungen über das specifische Gewicht, die Ausdehnung durch die Wärme und den Siedepunkt einiger Flüssigkeiten. *Pogg. Ann.*, **72**, 223–293.

Lacks, D. J. (1995). Origins of molar volume isotope effects in hydrocarbon systems. *J. Chem. Phys.*, **103**, 5085–5090.

Larson, A.C. & Von Dreele, R.B. (1994). General Structure Analysis System (GSAS). Los Alamos National Laboratory Report, LAUR 86-748.

Le Bail, A. (2005). Whole powder pattern decomposition methods and applications: A retrospection. *Powder Diff.*, **20**, 316–326.

Mantid (2013). Manipulation and Analysis Toolkit for Instrument Data; Mantid Project. http://dx.doi.org/10.5286/SOFTWARE/MANTID.

Meyer, J. (1910). Die Schmelzwärme der Essigsäure, des Benzols und des Nitrobenzols. *Z. Phys. Chem.*, **72**, 225–254.

Osugi, J., Shimizu, K., & Onodera, A. (1965). Liquid-solid transition at high pressure: benzene, monochlorobenzene and toluene. *Rev. Phys. Chem. Japan,* **34**, 97–101.

Salim, M. A., Willow, S. Y., & Hirata, S. (2016). Ice Ih anomalies: Thermal contraction, anomalous volume isotope effect, and pressure-induced amorphization. *J. Chem. Phys.*, **144**, article 204503.

Tammann, G. (1903). *Kristallisieren und Schmelzen*. Leipzig.

Toby, B.H. (2001). EXPGUI, a graphical user interface for GSAS. *J. Appl. Cryst.,* **34**, 210–213.

Tohji, K., & Murata, Y. (1982). X-ray Diffraction Study of the Melting of Benzene. *Jap. J. Appl. Phys.*, **21**, 1199–1204.

Umemoto, K., & Wentzcovitch, R. M. (2017). First principles study of volume isotope effects in ices VIII and X. *Jap. J. Appl. Phys.*, **56**, article 05FA03.

Umemoto, K., Sugimura, E., de Gironcoli, S., Nakajima, Y., Hirose, K., Ohishi, Y., & Wentzcovitch, R. M. (2015). Nature of the volume isotope effect in ice. *Phys. Rev. Lett.*, **115**, article 173005.

Van Hook, W. A. (1985). Isotope effects in condensed phases, the benzene example. Influence of anharmonicity; harmonic and anharmonic potential surfaces and their

isotope independence. Molar volume effects in isotopic benzenes. *J. Chem. Phys.,* **83**, 4107–4117.

van Laar, B., & Schenk, H. (2018). The development of powder profile refinement at the Reactor Centre Netherlands at Petten. *Acta Cryst. A* **74**, 88–92.

Wojciechowski, M. (1937). Measurement of certain physicochemical constants of benzene. *J. Res. Natl. Bur. Standards*. **19**, 347–352.

Ziegler, W. T., & Andrews, D. H. (1942). The heat capacity of benzene-d6. *J. Am. Chem. Soc.,* **64**, 2482–2485.